



# Astrocyte-derived neurons provide excitatory input to the adult striatal circuitry

Matthijs C. Dorst<sup>a,1</sup>, María Díaz-Moreno<sup>b,1</sup>, David O. Dias<sup>b</sup>, Eduardo L. Guimarães<sup>b</sup>, Daniel Holl<sup>b</sup>, Jannis Kalkitsas<sup>b</sup>, Gilad Silberberg<sup>a,2</sup>, and Christian Göritz<sup>b,c,2</sup>

<sup>a</sup>Department of Neuroscience, Karolinska Institutet, SE-171 77 Stockholm, Sweden; <sup>b</sup>Department of Cell and Molecular Biology, Karolinska Institutet, SE-171 77 Stockholm, Sweden; and <sup>c</sup>Ming Wai Lau Centre for Reparative Medicine, Stockholm Node, Karolinska Institutet, SE-17177 Stockholm, Sweden

Edited by Anders Björklund, Lund University, Lund, Sweden, and approved June 25, 2021 (received for review March 2, 2021)

**Astrocytes have emerged as a potential source for new neurons in the adult mammalian brain. In mice, adult striatal neurogenesis can be stimulated by local damage, which recruits striatal astrocytes into a neurogenic program by suppression of active Notch signaling (J. P. Magnusson et al., *Science* 346, 237–241 [2014]). Here, we induced adult striatal neurogenesis in the intact mouse brain by the inhibition of Notch signaling in astrocytes. We show that most striatal astrocyte-derived neurons are confined to the anterior medial striatum, do not express established striatal neuronal markers, and exhibit dendritic spines, which are atypical for striatal interneurons. In contrast to striatal neurons generated during development, which are GABAergic or cholinergic, most adult astrocyte-derived striatal neurons possess distinct electrophysiological properties, constituting the only glutamatergic striatal population. Astrocyte-derived neurons integrate into the adult striatal microcircuitry, both receiving and providing synaptic input. The glutamatergic nature of these neurons has the potential to provide excitatory input to the striatal circuitry and may represent an efficient strategy to compensate for reduced neuronal activity caused by aging or lesion-induced neuronal loss.**

astrocyte-derived neurogenesis | striatum | neurons | glutamatergic

The striatum is a central brain structure important for the initiation and coordination of motor functions, sensory processing, and reward (1–3). The striatal neuronal composition is dominated by a vast majority (~95%) of projection neurons, the so called medium spiny neurons (MSNs), and a small yet diverse population of interneurons. The vast majority of striatal neurons is GABAergic, apart from one population of cholinergic interneurons, which provide most of the cholinergic input to the network (4). GABAergic interneurons provide synaptic inhibition to MSNs with cell type-dependent characteristics such as the location of inhibitory synapses (MSN cell bodies or dendrites), synaptic dynamics (depression and facilitation), and connection probability (5). This intricate synaptic connectivity is essential for normal striatal function as it shapes the activity of MSNs, thus determining the downstream flow of information from the striatum to the output nuclei of the basal ganglia. There are several types of GABAergic interneurons, and their classification is an ongoing effort, facilitated by recently discovered, new types of neurons and neuronal markers (6–9).

Most striatal neurons are generated during early development. There is evidence for adult striatal neurogenesis in the uninjured human brain (10) and possibly some nonhuman primates and to a much smaller degree in rats and rabbits (11). For their abundance throughout the brain and similarity to adult neural stem cells, parenchymal astrocytes have emerged as a potential source for new neurons in nonneurogenic brain regions (12). Indeed, in response to experimental stroke or an excitotoxic lesion, some astrocytes in the mouse striatum can generate neurons (13–16). In both lesions striatal astrocytes are recruited into a neurogenic program (15, 16), which is mediated through suppression of active Notch signaling (15). Striatal neurogenesis in mice can also be evoked by deletion of the Notch downstream effector RBPj-κ

in astrocytes in the otherwise intact striatum (15) and offers a model system to study adult-born striatal neurons. Furthermore, deletion of RBPj-κ in striatal astrocytes in the context of stroke increases the efficacy of astrocyte recruitment and boosts stroke-induced striatal neurogenesis (17). Therapeutically interesting, adult neurogenesis by striatal astrocytes can be further amplified by epidermal growth factor infusion (18). However, it is currently unclear whether astrocyte-derived neurons become functional, which neuronal properties they possess, and whether they can integrate into the adult striatal circuitry.

To better understand the function of adult striatal neurogenesis and harness its therapeutic potential, we capitalized on the ability to induce astrocyte-derived striatal neurogenesis in the adult mouse brain by cell-specific inhibition of the Notch signaling pathway. We show that most astrocyte-derived neurons constitute a previously unknown subset of striatal neurons with distinct electrophysiological properties and morphological features, which possess the capacity to synaptically integrate into the adult striatal circuitry and provide glutamatergic input to striatal projection neurons.

## Results

We targeted astrocytes using previously established Connexin-30 (Cx30)-CreER<sup>T2</sup> transgenic mice (15, 19) carrying a Rosa26-tdTomato reporter allele (20) and conditional RBPj-κ null alleles

## Significance

**The adult mammalian brain has a poor regenerative capacity. Astrocytes have the potential to enter a neurogenic program, which could supply new neurons to the adult brain. In the adult striatum, reduced Notch signaling in astrocytes leads to the generation of neurons. However, it has been unclear whether striatal astrocyte-derived neurons become integrated and which neuronal properties they possess. Here, we show that induced adult neurogenesis by striatal astrocytes leads to the generation of glutamatergic neurons that functionally integrate into the adult striatal circuitry. The integration of glutamatergic neurons provides a local source of excitation to the striatum that could potentially compensate for reduced excitatory input due to aging or disease.**

Author contributions: M.C.D., M.D.-M., D.O.D., G.S., and C.G. designed research; M.C.D., M.D.-M., D.O.D., E.L.G., D.H., and J.K. performed research; M.C.D., M.D.-M., D.O.D., E.L.G., D.H., and J.K. analyzed data; M.C.D., D.O.D., G.S., and C.G. wrote the paper; and C.G. initiated, designed, and supervised the study.

The authors declare no competing interest.

This article is a PNAS Direct Submission.

Published under the PNAS license.

<sup>1</sup>M.C.D. and M.D.-M. contributed equally to this work.

<sup>2</sup>To whom correspondence may be addressed. Email: gilad.silberberg@ki.se or christian.goeritz@ki.se.

This article contains supporting information online at <https://www.pnas.org/lookup/suppl/doi:10.1073/pnas.2104119118/-DCSupplemental>.

Published August 13, 2021.

(21), hereafter referred to as Cx30-CreER<sup>T2</sup>; RBPj- $\kappa$ <sup>loxP/loxP</sup>; R26R-tdTom mice. These mice can be used to inhibit RBPj- $\kappa$ -dependent Notch signaling in adult astrocytes upon tamoxifen administration (SI Appendix, Fig. S1). As previously described, homozygous deletion of RBPj- $\kappa$  (RBPj- $\kappa$ <sup>fl/fl</sup>) induced a neurogenic program in medial striatal astrocytes, which led to the upregulation of the proneural transcription factor Ascl1, proliferation and the generation of neuroblasts, which consequently mature into NeuN<sup>+</sup> neurons (15, 18) (Fig. 1A). RBPj- $\kappa$  deletion does not cause migration of neuroblasts from the subventricular zone into the striatum (15). Heterozygous RBPj- $\kappa$ <sup>wt/fl</sup> mice do not undergo a neurogenic program in striatal astrocytes and served as control (15). We confirmed that the neurons were adult-born and astrocyte-derived by 5-ethynyl-2'-deoxyuridine (EdU) incorporation (22) and tdTomato expression, respectively (Fig. 1A and B). At 12 wk after RBPj- $\kappa$  deletion, most astrocyte-derived neurons were detected in the anterior medial striatum, reaching up to  $81.5 \pm 30.5$  cells per mm<sup>2</sup> ( $n = 4$  animals) in the most anterior part (Fig. 1C and D).

In order to classify the astrocyte-derived neurons, we applied a panel of known striatal neuron markers. While we found striatal neurons expressing the subtype markers dopamine- and cAMP-regulated phosphoprotein-32 (DARPP-32), choline acetyltransferase (ChAT), parvalbumin (PV), calretinin, calbindin, calmodulin, somatostatin, substance P receptor, and neuropeptide Y (NPY), none of the recombined cells expressed any of these markers (Fig. 1E and SI Appendix, Fig. S24). A small fraction ( $9 \pm 0.6\%$ ,  $n = 5$  animals) of astrocyte-derived neurons expressed neuronal nitric oxide synthase (nNOS), a marker for a subtype of GABAergic medium-sized striatal interneurons (Fig. 1F). For the remaining  $91\% \pm 0.6$  of NeuN<sup>+</sup> tdTomato<sup>+</sup> striatal neurons, we could not find a subtype-specific marker.

To characterize the electrophysiological properties of astrocyte-derived striatal neurons, we used whole-cell patch-clamp recordings in acute brain slices 12 to 16 wk after recombination induction (Fig. 2A and B). The electrophysiological characteristics of astrocyte-derived neurons differed significantly from neighboring recombined astrocytes, most notably in their higher input resistance ( $P < 0.001$ ,  $n = 27$  neurons, 35 astrocytes, independent  $t$  test) and longer membrane time constant ( $\tau_{\text{mem}}$ ) ( $n = 28$  neurons, 46 astrocytes). As a defining criterion for the electrophysiological classification as a neuron, we used action potential discharge (Fig. 2C–G). Some of the putative astrocyte-derived neurons did not discharge action potentials and differed from action potential discharging astrocyte-derived neurons in their high input resistance ( $1,248.5 \pm 251$  M $\Omega$ ,  $n = 14$ ) and depolarized resting membrane potential ( $-32.5 \pm 5.6$  mV,  $n = 14$ ) (SI Appendix, Fig. S3A–E). These neuron-like cells may represent an immature population still in transition and were, therefore, excluded from further analysis.

Next, we compared astrocyte-derived neurons with known striatal neuron subtypes. We found that astrocyte-derived neurons shared some characteristics with striatal low-threshold spiking (LTS) interneurons, including relatively small action potentials, a long membrane time constant, and a high input resistance. However, while LTS interneurons typically exhibit depolarized resting membrane potentials, astrocyte-derived neurons were more hyperpolarized ( $n = 22$  LTS interneurons, 28 astrocyte-derived neurons,  $P = 1.3351 \times 10^{-10}$ , independent  $t$  test; Fig. 2G and Table 1). Astrocyte-derived neurons exhibited a sag and rebound current which is typically found in cholinergic interneurons (ChINs); however, they differed from this population in other properties such as input resistance ( $P = 2.7219 \times 10^{-15}$ ,  $n = 10$  ChINs, 27 astrocyte-derived neurons, independent  $t$  test) and action potential amplitude ( $P = 2.8496 \times 10^{-7}$ ,  $n = 9$  ChINs, 27 astrocyte-derived neurons, independent  $t$  test). Astrocyte-derived neurons differed significantly from the common MSNs in their electrophysiological properties, including a more depolarized

resting membrane potential, deeper sag, longer time constant, and higher membrane resistance; astrocyte-derived neurons also exhibited a smaller soma compared to MSNs (SI Appendix, Fig. S3F and G). The amplitude of action potentials was smaller than that of other neurons ( $45 \pm 2$  mV and ranged from 25 to 69 mV; Fig. 2G and Table 1), which may indicate their earlier maturation stage. We therefore also compared astrocyte-derived neurons to striatal neurons recorded in preadolescent mice (aged postnatal week  $5 \pm 2$ ) to account for the difference in maturation (SI Appendix, Fig. S3H and I). Striatal neurons recorded in younger mice exhibited comparable electrophysiological characteristics as those recorded in adult mice and differed significantly in key properties from astrocyte-derived neurons. To characterize the morphology of astrocyte-derived neurons, we filled them with neurobiotin during electrophysiological recordings for subsequent staining and morphological reconstruction (Fig. 2H). Electrophysiologically defined neurons showed several neurites extending from the soma and branching thereafter. The longest neurites extended for up to 150  $\mu\text{m}$  before exiting the section plane. Interestingly, we found a substantial number of dendritic spines on all investigated neurons (Fig. 2H), which is atypical for striatal interneurons. Taken together, our results show that astrocyte-derived neurons constitute a population of striatal neurons, distinct from previously defined striatal neuronal subtypes.

We observed that a number of astrocyte-derived neurons received spontaneous synaptic input, likely arising from nearby spontaneously active neurons or projecting axons (Fig. 3A). The spontaneous activity was not affected by bath application of the GABA<sub>A</sub> receptor antagonist SR-95531 (gabazine 10  $\mu\text{M}$ ,  $P = 0.69$ ,  $n = 6$ , Wilcoxon signed-rank test) but reduced significantly following bath application of the AMPA receptor antagonist NBQX ( $P = 0.037$ ,  $n = 10$ , Wilcoxon signed-rank test), suggesting that these events were largely mediated by glutamatergic axon terminals (Fig. 3B). To further study synaptic input to astrocyte-derived neurons, we used an extracellular stimulation electrode to trigger action potentials in nearby neurons and axons and measured the response in whole-cell recorded astrocyte-derived neurons (Fig. 3C). Extracellular stimulation robustly triggered postsynaptic responses in astrocyte-derived neurons, which could be attenuated by gabazine, confirming their synaptic nature and demonstrating the presence of GABA<sub>A</sub> receptors on astrocyte-derived neurons (Fig. 3D).

To further investigate the synaptic integration of astrocyte-derived neurons, we crossed Cx30-CreER<sup>T2</sup>; RBPj- $\kappa$ <sup>loxP/loxP</sup> mice to the Rosa26-ChR2-tdTomato line, which allows Cre-dependent expression of a channelrhodopsin 2 (ChR2)/tdTomato fusion protein (23) upon tamoxifen-induced genetic recombination (Fig. 4A). In RBPj- $\kappa$ <sup>fl/fl</sup> mice, exposure to photostimulation with 473 nm blue light (200-ms pulse length) led to robust depolarization of astrocytes and astrocyte-derived neurons, with larger depolarization observed in astrocytes (Fig. 4B and C). To test for synaptic connections, brief light pulses (5 ms) were delivered, while whole-cell recordings were obtained from striatal MSNs. Photostimulation induced postsynaptic potentials in MSNs in the presence of astrocyte-derived neurons but not in RBPj- $\kappa$ <sup>wt/fl</sup> control mice, in which only astrocytes expressed ChR2 (Fig. 4D–G). In responding MSNs, bath application of gabazine reduced postsynaptic potential amplitudes by 26% (from  $4.8 \pm 2.8$  mV to  $3.5 \pm 2.1$  mV,  $P = 0.03$ ,  $n = 8$ , Wilcoxon signed-rank test), confirming the presence of a GABAergic component in the postsynaptic response (Fig. 4D and F). Surprisingly, bath application of the AMPA receptor antagonist NBQX (10  $\mu\text{M}$ ) strongly attenuated fast postsynaptic responses in all tested MSNs from  $5.3 \pm 3.1$  mV to  $0.3 \pm 0.1$  mV ( $P = 0.007$ ,  $n = 9$ , Wilcoxon signed-rank test). In a subset of experiments, further application of the NMDA receptor antagonist amino-5-phosphonopentanoate (AP5) abolished the remaining response (Fig. 4D). These data show that astrocyte-derived neurons

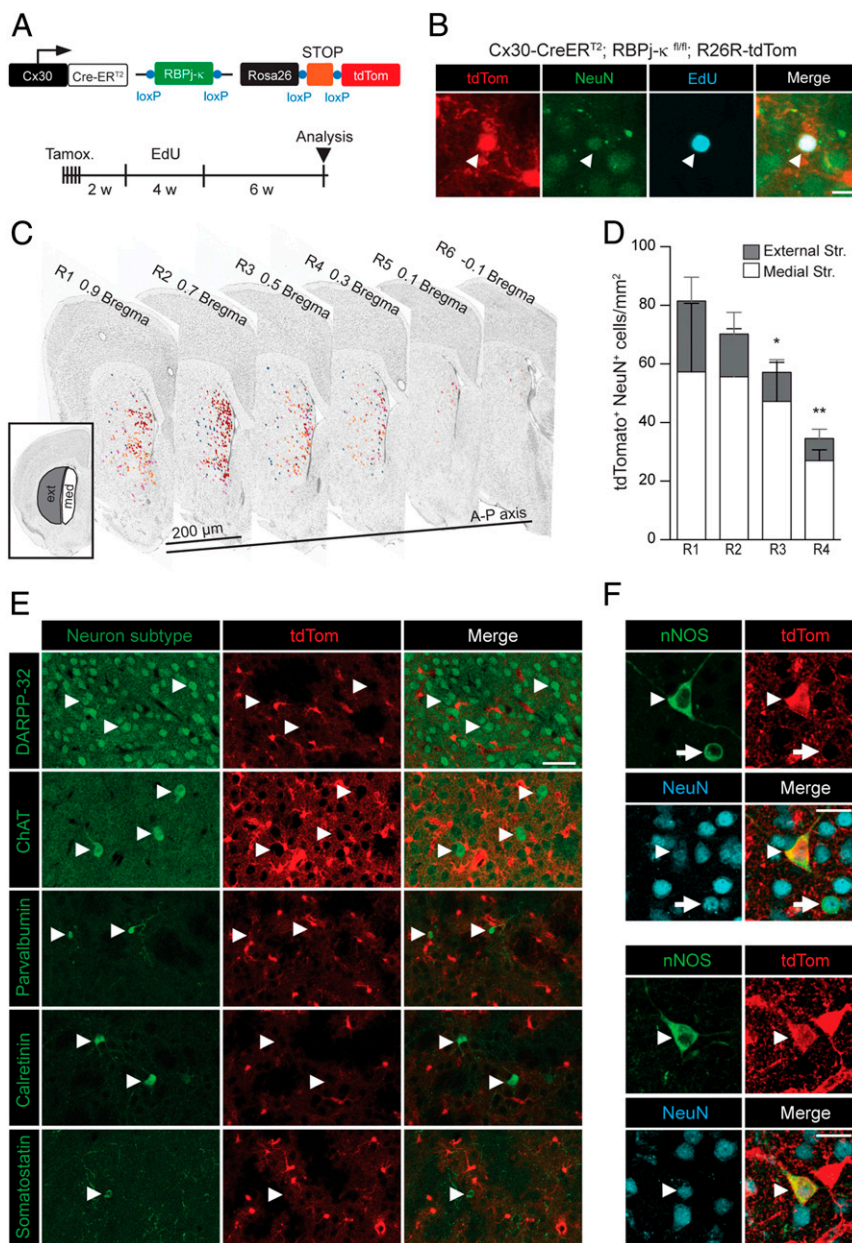


**Fig. 1.** Astrocyte-derived neurons are preferentially located in the anterior medial striatum. (A) Schematic of the transgenic mouse line and experimental outline of the study. Adult animals (8 wk-old) homozygous for the conditional *Rbpj-κ* gene were given tamoxifen for 5 consecutive d to induce selective ablation of *RBPj-κ* and reporter expression (tdTom, tdTomato) in astrocytes and their progeny. Two weeks after tamoxifen-mediated genetic recombination, animals received EdU via the drinking water for 4 wk, and brain tissue was collected for analyses 6 wk later (12 wk after *RBPj-κ* deletion). (B) Conditional homozygous deletion of *RBPj-κ* in adult Cx30-CreER<sup>T2</sup>-expressing striatal astrocytes leads to the production of adult-born neurons via proliferation. Arrowhead shows a recombined (tdTom<sup>+</sup>) astrocyte-derived neuron (NeuN<sup>+</sup>) that incorporated EdU. (C and D) Distribution (C) and quantification (D) of adult-born, astrocyte-derived neurons in the striatum along the anterior–posterior axis, from region 1 (R1) to R4. Each colored dot represents an adult-born, astrocyte-derived neuron. (E) Recombined striatal cells (tdTom<sup>+</sup>) do not express DARPP-32, ChAT, parvalbumin, calretinin, or somatostatin. Arrowheads point at striatal neurons positive for the neuron subtype marker and negative for tdTom. (F) A fraction of astrocyte-derived neurons (NeuN<sup>+</sup>/tdTom<sup>+</sup> cells; arrowheads) expresses nNOS. The arrow marks a nonrecombined nNOS-expressing striatal interneuron. (Scale bars, 10 μm [B], 50 μm [E], and 20 μm.) (F). Data shown as mean ± SEM ( $n = 4$  animals), \* $P = 0.0376$ , \*\* $P = 0.0074$  by independent  $t$  test (external versus medial striatum) in D.

are glutamatergic and that the GABAergic component may be the result of recruitment of local inhibitory neurons.

The peak delay for postsynaptic responses was unaffected by gabazine but slightly increased following application of NBQX ( $P = 0.05$ ,  $n = 9$ , Wilcoxon signed-rank test), suggesting the presence of a small residual NMDA component (Fig. 4F). Application of eight light pulses of 3 ms at 40 Hz produced strongly depressing

postsynaptic responses, indicating strong short-term depression or an inability to repeatedly trigger light-induced action potentials in presynaptic neurons (Fig. 4E). We also tested the existence of direct synaptic connections between astrocyte-derived neurons and neighboring MSNs using paired patch-clamp recordings; however, no direct connections were found in nine such pairs, suggesting that connectivity may be sparse or severed during slice preparation.

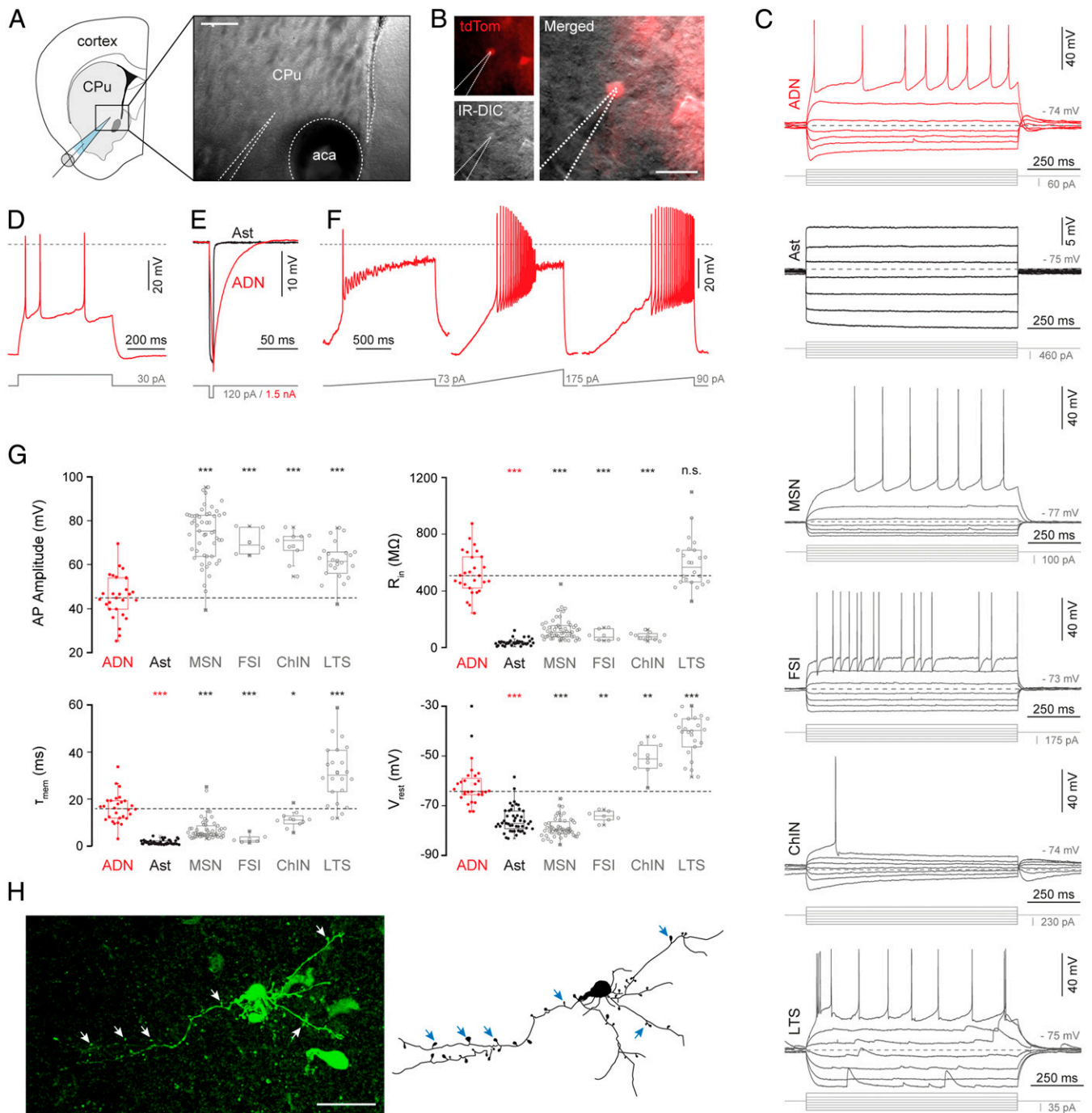


**Fig. 2.** Astrocyte-derived neurons have unique electrophysiological properties distinct from the major striatal neuron subtypes. (A) Adult-born, astrocyte-derived neurons were identified in the region surrounding the anterior commissure (aca) in the caudate putamen (CPu), lateral of the lateral ventricle. (B) Neurons were selected by their expression of tdTom and identified by their distinct morphology and electrophysiological properties. (C) Current-voltage responses of astrocyte-derived neurons (ADNs), astrocytes (ast), MSNs, FSIs, Cholinergic Interneurons (ChINs), and LTS interneurons. Dotted lines mark baseline membrane potential. (D) TdTom-expressing cells were classified as neurons based on their discharge of action potentials. (E) ADNs (red) have longer membrane time constants compared to astrocytes (black). (F) Examples from three different ADNs discharging action potentials in response to ramp current injections. (G) Distinct membrane properties reveal ADNs as a unique population unlike well-known caudal neurons, most notably by their shallow action potentials, input resistance ( $R_{in}$ ), and resting membrane potential ( $V_{rest}$ ). \* $P < 0.05$ , \*\* $P < 0.01$ , and \*\*\* $P < 0.001$  by independent  $t$  test for all comparisons (ADNs versus astrocytes, MSN, FSI, ChIN, or LTS interneurons). (H) Patched neurons were filled with neurobiotin for post hoc staining and morphological analysis. ADNs presented highly branched neurites and dendritic spines (arrows). Scale bars represent 250  $\mu$ m (A) and 25  $\mu$ m (B and H).

In line with our electrophysiological results, we detected expression of *Vglut1* mRNA (vesicular glutamate transporter 1, *Slc17a7*), an essential component for glutamate transport, in astrocyte-derived striatal neurons by in situ hybridization. In turn, *Vglut2* mRNA

(vesicular glutamate transporter 2, *Slc17a6*) signals were virtually absent in the striatum and in astrocyte-derived neurons (Fig. 4 H and I).

Together, our results show that apart from a small population of nNOS-expressing GABAergic interneurons, most astrocyte-derived

**Table 1. Electrophysiological properties of astrocyte-derived neurons**

	ADN ( <i>n</i> = 28)	Astrocyte ( <i>n</i> = 47)	MSN ( <i>n</i> = 52)	FSI ( <i>n</i> = 6)	ChIN ( <i>n</i> = 12)	LTS ( <i>n</i> = 22)
$V_{rest}$ (mV)	$-61.4 \pm 1.7$	$-75.8 \pm 0.7$	$-78.8 \pm 0.5$	$-74.2 \pm 1.0$	$-50.5 \pm 2.0$	$-41.5 \pm 1.7$
AP half width (ms)	$0.87 \pm 0.03$		$0.94 \pm 0.16$	$0.44 \pm 0.05$	$0.83 \pm 0.07$	$0.65 \pm 0.02$
AP amplitude (mV)	$45.3 \pm 1.9$		$73.7 \pm 1.7$	$70.2 \pm 2.4$	$63.0 \pm 5.3$	$61.6 \pm 1.8$
Sag amplitude (mV)	$6.5 \pm 0.5$	$0.3 \pm 0.1$	$2.25 \pm 0.36$	$1.44 \pm 0.51$	$9.43 \pm 0.71$	$5.10 \pm 0.94$
$R_{in}$ (M $\Omega$ m)	$522 \pm 29$	$36.1 \pm 3.9$	$128 \pm 11$	$86.3 \pm 17$	$90.5 \pm 17$	$596 \pm 38$
$\tau_{mem}$ (ms)	$16.1 \pm 1.2$	$1.63 \pm 0.14$	$7.2 \pm 0.6$	$3.01 \pm 0.75$	$12.0 \pm 2.3$	$31.1 \pm 2.6$

Astrocyte-derived neuron (ADN), medium spiny neuron (MSN), fast-spiking interneuron (FSI), cholinergic interneuron (ChIN), low-threshold spiking (LTS). Data are presented as mean  $\pm$  SEM.

neurons are glutamatergic, possess characteristic neuronal properties, and integrate into the striatal circuitry by both receiving and providing synaptic input.

## Discussion

The discovery of adult neurogenesis and the possibility to add new neurons to the adult brain has stimulated great interest regarding its functions and therapeutic potential. There is evidence that adult hippocampal neurogenesis may occur to a similar extent in humans and mice (24). The study of this process in rodents has led to the establishment of its role in pattern separation-dependent memory (25–27), and its dysregulation has been linked to psychiatric disorders (28, 29).

Based on carbon<sup>14</sup> retrospective birth dating, the extent of adult hippocampal and striatal neurogenesis is comparable in humans (11), suggesting a functional significance for adult-born striatal neurons. Previous studies in humans and rabbits identified calretinin as a positive marker for a larger proportion of newborn striatal neurons (10, 30). However, calretinin expression in the striatum is highly species dependent and much higher in primates compared to rodents (31, 32). Furthermore, calretinin does not define a unique striatal interneuron subclass either (7, 33) and may only be transiently expressed in new striatal interneurons, as described for adult-born dentate gyrus granule cells (34). The total number of calretinin-expressing neurons peaks during postnatal development and then declines (35), suggesting that calretinin expression may in fact be transient in some immature striatal populations.

In mice, adult striatal neurogenesis occurs in response to striatal lesions, indicating a role in the endogenous repair process. Following a lesion to the striatum, Notch signaling is downregulated in local astrocytes, which induces their recruitment into a neurogenic program (15, 18). Here, we took advantage of this mechanism to generate adult-born, astrocyte-derived, striatal neurons in the uninjured mouse striatum by genetic deletion of the Notch effector RBPj- $\kappa$  in astrocytes. The vast majority of astrocyte-derived striatal neurons did not acquire characteristics of previously described neuronal subtypes in the striatum but instead differentiated into glutamatergic, spine-forming neurons. While all astrocyte-derived neurons expressed the mature neuronal marker NeuN, only a fraction was immunopositive for the striatal interneuron marker nNOS. This is in line with our previous study, in which, after stroke, we could only identify nNOS as a subtype-specific marker for some astrocyte-derived striatal neurons (15). Since stroke-induced astrocyte neurogenesis occurs via a mechanism dependent on decreased Notch signaling (15), it is plausible that neurons generated by RBPj- $\kappa$  deletion in striatal astrocytes in the uninjured brain share some characteristics to the ones generated after stroke.

Notch signaling plays a critical role in neural stem and progenitor cell maintenance during development. Depletion of Notch signaling activates neurogenic differentiation programs in radial glial cells (36). RBPj- $\kappa$ -mediated canonical Notch signaling regulates the expression of the target genes *Hes1* and *Hes5*, which can negatively control the expression of the proneural genes *Ascl1*, *Neurog1*, and *Neurog2* (37–40). Apart from their

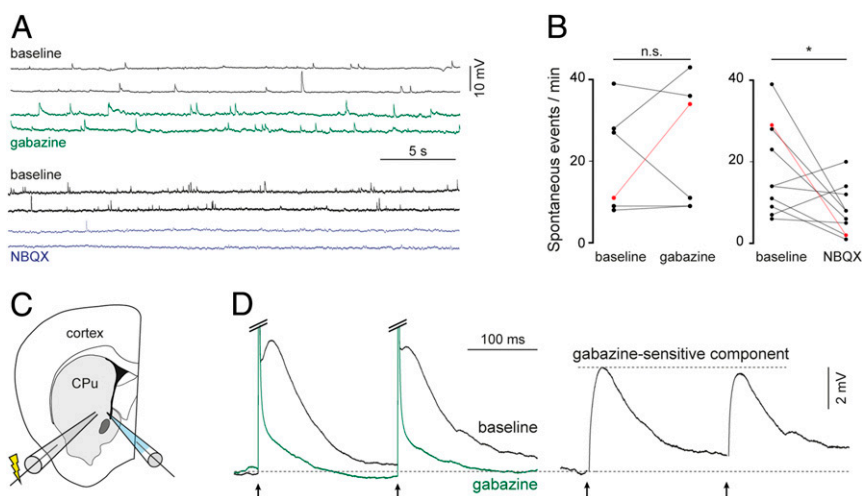


**Fig. 3.** Astrocyte-derived neurons receive GABAergic and glutamatergic input. (A and B) Spontaneous postsynaptic events observed in astrocyte-derived neurons were not affected by gabazine (*n* = 6 responding neurons,  $Z = -0.405$ ,  $P = 0.686$ ) but reduced in the presence of NBQX (*n* = 10 responding neurons,  $Z = -2.090$ ,  $P = 0.037$ , Wilcoxon signed-rank test). Data points marked in red (B) correspond to example traces in A. (C and D) An extracellular stimulation electrode (C) was used to trigger postsynaptic responses in astrocyte-derived neurons. (D, Right) Synaptic responses in the presence of gabazine subtracted from responses under control conditions reveal a large GABA-mediated component.

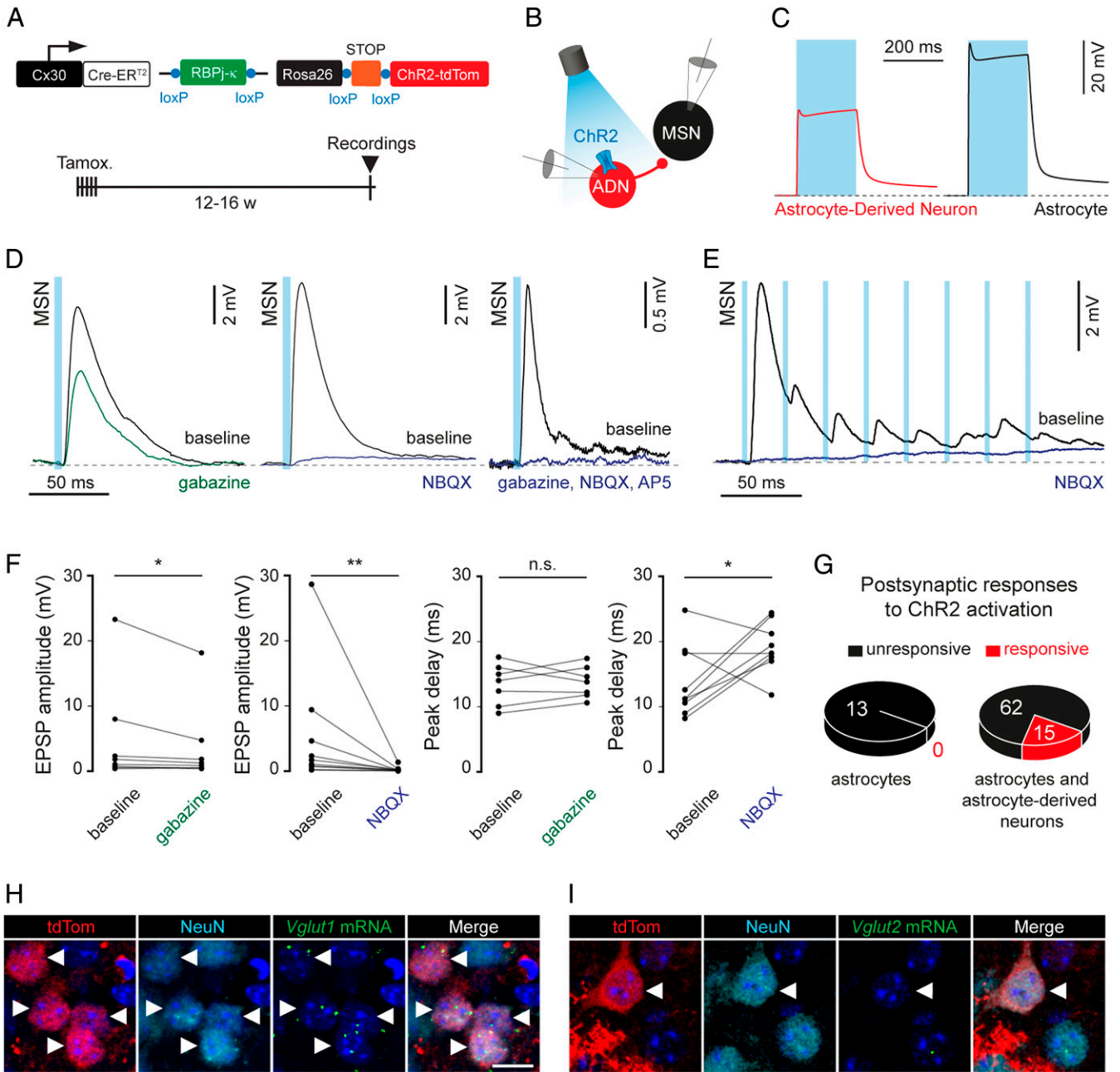


**Fig. 4.** Astrocyte-derived neurons are glutamatergic and functionally connect to nearby MSNs. (A–C) In mice crossed with a ChR2-tdTom reporter (A), astrocyte-derived neurons and astrocytes (B) exhibit a clear light-induced depolarization (C). (D) Postsynaptic responses in MSNs induced by a 5-ms light pulse were attenuated by gabazine (10  $\mu$ M) and strongly reduced by NBQX (10  $\mu$ M). In a subset of experiments, the additional application of NBQX and amino-5-phosphonopentanoate (AP5) abolished postsynaptic responses completely. (E) A 40 Hz train of 3-ms light pulses produced sharply depressing postsynaptic responses. (F) Light-induced responses were reduced in amplitude in the presence of gabazine ( $P = 0.03$ ,  $n = 8$  responding neurons) and more strongly reduced in the presence of NBQX ( $P = 0.007$ ,  $n = 9$  responding neurons). Peak delay was unaffected by gabazine ( $P = 0.87$ ,  $n = 7$  responding neurons) but increased in NBQX ( $P = 0.05$ ,  $n = 9$  responding neurons, Wilcoxon signed-rank test for all comparisons). (G) Fast postsynaptic responses to light activation were detected in mice expressing ChR2 in astrocytes and astrocyte-derived neurons (ADNs) ( $n = 13$  mice) but not in mice expressing ChR2 exclusively in astrocytes ( $n = 2$  mice). (H and I) Detection of *Vglut1* (*Slc17a7*) mRNA in astrocyte-derived striatal neurons (tdTom<sup>+</sup>/NeuN<sup>+</sup> cells, arrowheads) by RNAscope in situ hybridization combined with immunofluorescence for NeuN and tdTomato (H). Note that in the striatum, *Vglut1* mRNA signals in astrocyte-derived neurons are weaker than in glutamatergic excitatory neurons of the cerebral cortex. *Vglut2* (*Slc17a6*) mRNA signals are virtually absent in astrocyte-derived striatal neurons (I). Cell nuclei are labeled with DAPI (blue). (Scale bar, 10  $\mu$ m.)

established function in specification of neural progenitor cells, proneural genes can also regulate neuronal-subtype differentiation programs (37). Similar to neural stem cells during development, decreased Notch signaling in striatal astrocytes leads to up-regulation of *Ascl1* and *Neurog1* (18). In the adult sub-ventricular zone, *Ascl1* and *Pax6* are co-expressed by neural

precursors that generate GABAergic olfactory bulb interneurons but also specify glutamatergic lineage when expressed along *Neurog2* and the T-box brain genes *Tbr2* (also known as *Eomes*) and *Tbr1* (41, 42). With some exceptions, where it can regulate GABAergic fate, *Neurog1* has been implicated in glutamatergic lineage specification in most brain regions. For example, during

cortical development *Neurog1* and *Neurog2* play important roles in the specification of lower-layer glutamatergic cortical projection neurons, with concomitant repression of subcortical GABAergic neuronal fate (43). In the dorsal telencephalon, *Neurog1* and *Neurog2* are critical to instruct glutamatergic fate through activation of the downstream transcription factors *NeuroD*, *Tbr2* and *Tbr1* (44–46). These findings suggest that *Neurog1* and *Ascl1* may interact with other transcription factors to determine neurotransmitter identities of astrocyte-derived neurons.

We found that most astrocyte-derived neurons do not express established striatal neuronal markers. In line with this, astrocyte-derived neurons showed unique neuronal electrophysiological properties compared to previously characterized neuronal subtypes in the striatum. The glutamatergic nature of astrocyte-derived striatal neurons is intriguing, as apart from cholinergic interneurons, all other known types of striatal neurons are GABAergic. Moreover, the appearance of dendritic spines adds further evidence that this population is distinct from previously characterized striatal interneurons (47). Adult-born granule cells added to the dentate gyrus and olfactory bulb share similar molecular markers to granule cells established during embryonic development (48, 49). The glutamatergic nature of astrocyte-derived neurons in the inhibitory striatal circuitry is, therefore, unexpected.

We identified a number of immature astrocyte-derived neurons, which showed higher membrane resistance and a more depolarized resting potential compared to mature astrocyte-derived neurons, indicating that they still lack the ion channels necessary to fire action potentials (*SI Appendix, Fig. S3*). Among the astrocyte-derived neurons that exhibited action potentials, we only observed minor differences in action potential amplitudes and firing rates, which may indicate further stages of maturation.

Most importantly, we found that astrocyte-derived neurons synaptically integrated into the adult striatal circuitry, both as pre- and postsynaptic counterparts. Commonly, the striatum receives glutamatergic input that originates from cortex and thalamus. The integration of glutamatergic neurons into the adult striatum introduces a local source of excitatory input to the striatal circuitry. This may represent an efficient way to compensate for decreased neuronal activity caused by neuronal loss due to aging, neurodegeneration, or injury. It may also present a plasticity mechanism for fine-tuning striatal activity in adulthood. Further studies could elucidate the specific functional roles of astrocyte-derived neurons in striatal function.

## Materials and Methods

**Transgenic Mice.** Connexin 30 (Cx30; official gene symbol *Gjb6*)-CreER<sup>T2</sup> transgenic mice (19) were crossed to the Rosa26-tdTomato (tdTom) Cre-reporter line (obtained from the Jackson Laboratory, B6.Cg-Gt(Rosa)26Sor<sup>tm14(CAG-tdTomato)Hze/J</sup>, Ai14, JAX stock: 007914) (20) to generate Cx30-CreER<sup>T2</sup>;R26R-tdTom mice, in which CreER<sup>T2</sup> is hemizygous and Rosa26-tdTom is either heterozygous or homozygous. Cx30-CreER<sup>T2</sup>;R26R-tdTom mice were further crossed to RBPj-κ<sup>loxP/loxP</sup> mice (21) to obtain Cx30-CreER<sup>T2</sup>; RBPj-κ<sup>loxP/loxP</sup>; R26R-tdTom mice, carrying Rbpj-κ<sup>w<sup>fl</sup></sup> or Rbpj-κ<sup>fl/fl</sup> genes.

For electrophysiology experiments combined with optogenetic stimulation, Cx30-CreER<sup>T2</sup>; RBPj-κ<sup>loxP/loxP</sup> animals were crossed to the Rosa26-ChR2-tdTomato Cre-reporter line (obtained from the Jackson Laboratory, B6.Cg-Gt(Rosa)26Sor<sup>tm27.1(CAG-COP4\*H123R/tdTomato)Hze/J</sup>, Ai27D, JAX stock: 012567) (23) to generate Cx30-CreER<sup>T2</sup>; RBPj-κ<sup>loxP/loxP</sup>; R26R-ChR2-tdTom mice, in which CreER<sup>T2</sup> is hemizygous, Rosa26-ChR2-tdTom is either heterozygous or homozygous, and Rbpj-κ is either heterozygous or homozygous.

Electrophysiological recordings in preadolescent controls were performed in heterozygous Lhx6-eGFP (obtained from the Mutant Mouse Resource and Research Center [MMRRC], stock number: 000246-MU) mice in which both fast-spiking interneurons (FSIs) and low-threshold spiking (LTS) interneurons are labeled with eGFP or in heterozygous PV-Cre mice (obtained from the Jackson Laboratory, B6.129P2-Pvalb<sup>tm1(Cre)Arb/J</sup>, JAX stock: 017320) crossed to a homozygous Rosa26-tdTomato Cre-reporter line (obtained from the

Jackson Laboratory, B6.Cg-Gt(Rosa)26Sor<sup>tm9(CAG-tdTomato)Hze/J</sup>, Ai9, JAX stock: 007909) to label FSIs. Lhx6-eGFP mice were in a Swiss Webster background (RjOrl:SWISS, Janvier). Preadolescent controls were recorded in mice aged 5 ± 2 wk old.

Unless otherwise specified, mice were in a C57BL/6J genetic background and older than 8 wk of age at the beginning of experiments. Mice were group-housed in a pathogen-free animal facility under controlled temperature and humidity and were kept on a 12:12-h light:dark cycle, with unrestricted access to food and water, as previously described (50). Both female and male animals were used. All experiments involving animals were performed according to the European Union and Swedish guidelines and approved by the institutional ethical committee (Stockholms Norra Djurförsöksetiska Nämnd).

**Genetic Labeling of Transgenic Mice.** Genetic recombination was induced by intraperitoneal injection of 2 mg tamoxifen per day (Sigma-Aldrich, T5648; 20 mg/mL in 1:9 EtOH:corn oil) for 5 consecutive d, as previously described (50). Animals were euthanized 12 wk and 12 to 16 wk after the last tamoxifen injection for immunofluorescence analyses and electrophysiology experiments, respectively.

**EdU Administration.** Two weeks after tamoxifen-mediated genetic recombination in Cx30-CreER<sup>T2</sup>; RBPj-κ<sup>fl/fl</sup>; R26R-tdTom mice, a cohort of animals (*n* = 4) received EdU for 4 wk via the drinking water (5-ethynyl-2'-deoxyuridine; 0.2 mg/mL supplemented with 1% sucrose, replaced every 2 to 3 d and kept in the dark), as previously described (50). Brain tissue was collected for analyses 6 wk later (12 wk after RBPj-κ deletion) in order to identify newly born astrocyte-derived neurons.

**Immunohistochemistry.** Animals were euthanized with an overdose of sodium pentobarbital. After ensuring the absence of a tail pinch response and pedal withdrawal reflex, animals were transcardially perfused with ice-cold phosphate-buffered saline (PBS) and then with 4% formaldehyde in PBS, as previously described (50). Brains were dissected out and immersed in 4% formaldehyde in PBS overnight at 4 °C. A Leica VT1000 S vibrating blade microtome was used to produce coronal brain sections (30 μm).

Tissue sections were first treated with blocking solution (10% normal donkey serum [NDS], supplemented with 0.3% Triton X-100 in PBS) for 1 h at room temperature (RT). After, sections were incubated with primary antibodies diluted in 10% NDS at RT overnight in a humidified chamber. The primary antibodies used for immunohistochemistry were the following: glutamine synthetase (1:2,000, rabbit, Invitrogen, PA1-46165), aldolase C (1:500, rabbit, Atlas Antibodies, HPA003282), aldehyde dehydrogenase 1 family member L1 (ALDH1L1; 1:500, rabbit, abcam, ab87117), S100β (1:500, guinea pig, Synaptic Systems, 287004), NeuN (1:500, mouse, Millipore, MAB377; 1:1,000, guinea pig, Millipore, ABN90), nNOS (1:300, goat, abcam, ab1376), substance P receptor (1:200, rabbit, Millipore, AB5060), somatostatin (1:500, rat, Millipore, MAB354), calmodulin (1:1,000, rabbit, Swant, 465), calbindin D28K (1:10,000, rabbit, Swant, CB38), calcitonin (1:2,000, rabbit, Swant, 7699/4), parvalbumin (1:5,000, rabbit, Swant, PV25; 1:100, guinea pig, Synaptic Systems, 195004), ChAT (1:100, goat, Millipore, AB144P; 1:1,000, sheep, abcam, ab18736), DARPP-32 (1:500, rabbit, Millipore, AB1656), and NPY (1:2,000, rabbit, Immunostar, 22940). A Monoclonal Antibody Labeling kit (Life Technologies) was used to directly conjugate Alexa Fluor 647 to the NeuN antibody from Millipore (clone A60). After washing in PBS, the following species-specific, fluorophore-conjugated secondary antibodies were used to reveal antibody staining (1:500; Cy3, Alexa Fluor 488, Alexa Fluor 647, and DyLight 405 from Jackson ImmunoResearch). Cell nuclei were marked with 4'6'-diamidino-2-phenylindole (DAPI) (1 μg/mL, Sigma-Aldrich, D9542). EdU was revealed using the Click-iT EdU Alexa Fluor 647 imaging kit (Life Technologies, C10340) following the manufacturer's specifications. To control for nonspecific signals, tissue sections were incubated with secondary antibodies alone. Sections were coverslipped with Antifade Mounting Medium (VECTA-SHIELD, Vector Labs, H-1000).

**RNAscope In Situ Hybridization.** For the detection of vesicular glutamate transporter 1 (*Slc17a7*) and vesicular glutamate transporter 2 (*Slc17a6*) RNA molecules, we performed RNAscope on formaldehyde-fixed tissue samples. Mice were first euthanized with an overdose of sodium pentobarbital, followed by transcardial perfusion with ice-cold PBS and 4% formaldehyde in PBS, as previously described (50). Brains were then postfixed in 4% formaldehyde in PBS for 6 h at 4 °C and dissected out. Coronal sections (30 μm-thick) were obtained using a vibratome (Leica VT1000 S vibrating blade microtome) and stored at 4 °C. In situ hybridization was performed following a modified version of the RNAscope Multiplex Fluorescent Reagent Kit version 2 Assay (ACD Bio-Techne, 323100).

In short, tissue sections were mounted onto SuperFrost Plus adhesion slides and baked for 30 min at 60 °C, prior to postfixation in 4% formaldehyde in PBS for 15 min at 4 °C. Slides were subsequently dehydrated in 50%, 70%, and 100% ethanol for 5 min each at RT. After drying, slides were first boiled for 10 s in distilled water followed by 5 min in antigen retrieval solution, washed in distilled water and 100% ethanol at RT, and allowed to dry again. For further antigen accessibility sections were incubated with protease III (ACD, 322337) at 40 °C for 30 min. For the RNAscope assay, the samples were washed in distilled water and incubated at 40 °C for 2 h with the following probes: Mm-Slc17a7 (ACD Bio-Techne, 416631) and Mm-Slc17a6-C2 (ACD Bio-Techne, 319171-C2). Subsequent amplification and detection were performed following the assay protocol. Probes were detected with Opal 520 fluorophore (Perkin-Elmer, FP1487A), followed by immunohistochemistry for NeuN (1:1,000, guinea pig, Millipore, ABN90) and Red Fluorescent Protein (1:500, rabbit, Rockland, 600-401-379; 1:500, chicken, Novus Biologicals, NBP1-97371) to recover tdTomato labeling. Cell nuclei were marked with DAPI (1 µg/mL, Sigma-Aldrich, D9542), and the sections were coverslipped with ProLong Gold antifade mountant (Invitrogen, P10144). The protocol was run in one day to preserve sample quality.

**Microscopy and Quantitative Analysis.** Images were taken using a Zeiss Axio-plan 2 upright epifluorescent microscope or a Leica TCS SP8X confocal microscope equipped with Leica Application Suite X software. Images were processed and assembled using ImageJ/Fiji (version 2.0.0-rc-43/1.51j for Mac), Adobe Photoshop CC 2019 20.0.9 release, and Illustrator CC 2019 23.1.1 release for Mac.

All quantifications were performed in 30 µm coronal brain sections spanning rostrocaudal levels 0.9 mm to 0.3 mm anterior of bregma. For calculation of striatal astrocyte-derived neurons per area, the number of tdTom<sup>+</sup>/NeuN<sup>+</sup> cells in the medial and external striata were assessed in four alternate sections (denoted as regions 1 through 4 [R1 through R4]) per animal and was divided by the area of the medial and external striata, respectively.

The relative proportion of astrocyte-derived neurons (tdTom<sup>+</sup>/NeuN<sup>+</sup> cells) which co-expressed nNOS was assessed in four alternate sections per animal and presented as a percentage of total tdTom<sup>+</sup>/NeuN<sup>+</sup> cells.

NeuroLucida neuron tracing software (MBF Bioscience) was used to reconstruct the neurites of representative striatal astrocyte-derived neurons.

#### Electrophysiological Recordings and Optogenetic Stimulation.

**Slice preparation.** Whole-cell patch-clamp recordings were obtained from *ex vivo* brain slices. Transgenic animals were anesthetized with isoflurane (VM Pharma AB, Sweden) and decapitated, whereupon the brain was removed in ice-cold cutting solution containing (in millimolar): KCl 2.5, NaH<sub>2</sub>PO<sub>4</sub> · H<sub>2</sub>O 1.25, CaCl<sub>2</sub> · 2H<sub>2</sub>O 0.5, MgCl<sub>2</sub> · 6H<sub>2</sub>O 7.5, Glucose 10, NaHCO<sub>3</sub> 25, and Sucrose 205. Coronal sections of 250 µm thickness were cut using a VT1200S Vibratome (Leica, Japan) and subsequently left to recover for 30 min at 35 °C in artificial cerebrospinal fluid (ACSF) containing (in millimolar): NaCl 125, KCl 2.5, MgCl<sub>2</sub> · 6H<sub>2</sub>O 1, NaH<sub>2</sub>PO<sub>4</sub> · H<sub>2</sub>O 1.25, CaCl<sub>2</sub> · 2H<sub>2</sub>O 2, Glucose 25, and NaHCO<sub>3</sub> 25. Slices were maintained at RT from recovery until recording at 35 °C. Cutting solution and ACSF were continuously infused with carbogen (95% O<sub>2</sub>, 5% CO<sub>2</sub>) throughout the procedure. The recording chamber was continuously perfused with fresh carbogenated ACSF at 2 ml/min.

**Patch-clamp recordings and optogenetic stimulation.** Borosilicate glass pipettes were pulled using a P1000 Micropipette Puller (Sutter Instrument) for a resistance of 5 to 9 MΩ and filled with a depolarizing chloride intracellular

solution containing (in millimolar): K-gluconate 105, KCl 30, Na<sub>2</sub>-Phosphocreatine 10, Hepes 10, ATP-Mg 4, and GTP-Na 0.3. For post hoc staining, 0.1% neurobiotin was added to the intracellular solution in a subset of experiments. Astrocyte-derived neurons were selected by tdTomato expression and their apparent morphology under widefield fluorescent imaging and patched using Infrared-Differential Interference Contrast (IR-DIC) imaging on a BX51WI (Olympus, Japan) upright microscope using a 40× long-working-distance immersion objective. Widefield illumination was provided by an X-Cite 120 Q mercury arc lamp (Olympus, Japan). Putative neurons were targeted based on the absence of the dense network of processes typical for astrocytes. Cholinergic interneurons and FSIs were targeted based on their relatively large somata under IR-DIC imaging. LTS interneurons were recorded from transgenic Lhx6-eGFP (Gene Expression Nervous System Atlas [GENSAT] project) age-matched controls. In all cases, neural identity was confirmed by comparison to established electrophysiological properties.

Soma size was determined by manual tracing of the soma circumference under IR-DIC imaging using the ImageJ freehand selection tool (ImageJ version 1.48, NIH).

Once a whole-cell recording was achieved, a fixed current was injected to maintain membrane potential near -75 mV in current-clamp mode on a MultiClamp 700B (Molecular Devices). Responses to current steps were filtered at 2 kHz and digitized at 10 kHz on an ITC-18 (HEKA) and acquired with Igor Pro-6.3 (Wavemetrics). For optogenetic experiments, afferent fibers were stimulated through an ocular-mounted blue light-emitting diode (LED) producing 6.4 mW/mm<sup>2</sup> light under the objective, controlled through an SLA-1200-2 LED driver (Mightex). Baseline responses were recorded without receptor antagonists present in the ACSF. Response amplitude was calculated as maximum deflection from the 100-ms average preceding stimulation during a 25-ms window following light onset. Peak delay was calculated as time to reach peak response amplitude from light onset. For extracellular stimulation, an Iso-Flex stimulus isolator (A.M.P.I., Israel) produced a 0.3-ms current pulse through a large-diameter glass pipette tuned between 0.4 and 1.0 mA in order to reliably evoke synaptic input from a distance of ~150 µm to the nearest patched neuron. Light- and stimulus-evoked responses were averaged per cell with at least 10 repetitions for each condition.

**Statistical Analysis.** Data are presented as mean ± SEM. Sample sizes (n)/number of biological replicates, statistical methods employed, and corresponding *P* values are specified in the text and in the legend of the respective figure. *P* values below 0.05 were considered as statistically significant. Statistical analyses were performed in GraphPad Prism (version 6.0g for Mac) or SPSS Statistics 17.0 (IBM).

**Data Availability.** All study data are included in the article and/or *SI Appendix*.

**ACKNOWLEDGMENTS.** We thank Jonas Frisén, Jens P. Magnusson, and members of the C.G. and G.S. laboratories for valuable comments on the manuscript. C.G. is a Hållsten Academy Fellow, and both C.G. and G.S. are Knut and Alice Wallenberg (KAW) Academy Fellows. This study was supported by the Swedish Research Council (C.G. and G.S.), the Swedish Brain Foundation (C.G. and G.S.), the Ming Wai Lau Centre for Reparative Medicine (C.G.), the European Union Joint Programme - Neurodegenerative Disease (JPND) Deciphering Interactions of Acquired Risk Factors and ApoE-mediated Pathways in Alzheimer's Disease (DACAP-AD) (C.G.), the Wings for Life Foundation (C.G.), the KAW Foundation (C.G. and G.S.), and the strategic networks for neuroscience and stem cells and regenerative medicine at Karolinska Institutet (C.G. and G.S.).

1. A. M. Graybiel, Habits, rituals, and the evaluative brain. *Annu. Rev. Neurosci.* **31**, 359–387 (2008).
2. G. E. Alexander, M. D. Crutcher, Functional architecture of basal ganglia circuits: Neural substrates of parallel processing. *Trends Neurosci.* **13**, 266–271 (1990).
3. B. W. Balleine, M. R. Delgado, O. Hikosaka, The role of the dorsal striatum in reward and decision-making. *J. Neurosci.* **27**, 8161–8165 (2007).
4. Y. Kawaguchi, C. J. Wilson, S. J. Augood, P. C. Emson, Striatal interneurons: Chemical, physiological and morphological characterization. *Trends Neurosci.* **18**, 527–535 (1995).
5. H. Planert, S. N. Szydlowski, J. J. Hjorth, S. Grillner, G. Silberberg, Dynamics of synaptic transmission between fast-spiking interneurons and striatal projection neurons of the direct and indirect pathways. *J. Neurosci.* **30**, 3499–3507 (2010).
6. O. Ibáñez-Sandoval *et al.*, Electrophysiological and morphological characteristics and synaptic connectivity of tyrosine hydroxylase-expressing neurons in adult mouse striatum. *J. Neurosci.* **30**, 6999–7016 (2010).
7. J. M. Tepper, F. Tecuapetla, T. Koós, O. Ibáñez-Sandoval, Heterogeneity and diversity of striatal GABAergic interneurons. *Front. Neuroanat.* **4**, 150 (2010).
8. G. Silberberg, J. P. Bolam, Local and afferent synaptic pathways in the striatal microcircuitry. *Curr. Opin. Neurobiol.* **33**, 182–187 (2015).
9. A. B. Muñoz-Manchado *et al.*, Novel striatal GABAergic interneuron populations labeled in the 5HT3a(EGFP) mouse. *Cereb. Cortex* **26**, 96–105 (2016).
10. A. Ernst *et al.*, Neurogenesis in the striatum of the adult human brain. *Cell* **156**, 1072–1083 (2014).
11. A. Ernst, J. Frisén, Adult neurogenesis in humans—common and unique traits in mammals. *PLoS Biol.* **13**, e1002045 (2015).
12. M. Zamboni, E. Llorens-Bobadilla, J. P. Magnusson, J. Frisén, A widespread neurogenic potential of neocortical astrocytes is induced by injury. *Cell Stem Cell* **27**, 605–617.e5 (2020).
13. J. M. Parent, Z. S. Vexler, C. Gong, N. Derugin, D. M. Ferriero, Rat forebrain neurogenesis and striatal neuron replacement after focal stroke. *Ann. Neurol.* **52**, 802–813 (2002).
14. A. Arvidsson, T. Collin, D. Kirik, Z. Kokaia, O. Lindvall, Neuronal replacement from endogenous precursors in the adult brain after stroke. *Nat. Med.* **8**, 963–970 (2002).
15. J. P. Magnusson *et al.*, A latent neurogenic program in astrocytes regulated by Notch signaling in the mouse. *Science* **346**, 237–241 (2014).

16. G. Nato *et al.*, Striatal astrocytes produce neuroblasts in an excitotoxic model of Huntington's disease. *Development* **142**, 840–845 (2015).
17. G. Santopolo, J. P. Magnusson, O. Lindvall, Z. Kokaia, J. Frisén, Blocking Notch-signaling increases neurogenesis in the striatum after stroke. *Cells* **9**, 1732 (2020).
18. J. P. Magnusson *et al.*, Activation of a neural stem cell transcriptional program in parenchymal astrocytes. *eLife* **9**, e59733 (2020).
19. M. Slezak *et al.*, Transgenic mice for conditional gene manipulation in astroglial cells. *Glia* **55**, 1565–1576 (2007).
20. L. Madisen *et al.*, A robust and high-throughput Cre reporting and characterization system for the whole mouse brain. *Nat. Neurosci.* **13**, 133–140 (2010).
21. K. Tanigaki *et al.*, Notch-RBP-J signaling is involved in cell fate determination of marginal zone B cells. *Nat. Immunol.* **3**, 443–450 (2002).
22. A. Salic, T. J. Mitchison, A chemical method for fast and sensitive detection of DNA synthesis in vivo. *Proc. Natl. Acad. Sci. U.S.A.* **105**, 2415–2420 (2008).
23. L. Madisen *et al.*, A toolbox of Cre-dependent optogenetic transgenic mice for light-induced activation and silencing. *Nat. Neurosci.* **15**, 793–802 (2012).
24. K. L. Spalding *et al.*, Dynamics of hippocampal neurogenesis in adult humans. *Cell* **153**, 1219–1227 (2013).
25. C. D. Clelland *et al.*, A functional role for adult hippocampal neurogenesis in spatial pattern separation. *Science* **325**, 210–213 (2009).
26. T. Nakashiba *et al.*, Young dentate granule cells mediate pattern separation, whereas old granule cells facilitate pattern completion. *Cell* **149**, 188–201 (2012).
27. A. Sahay *et al.*, Increasing adult hippocampal neurogenesis is sufficient to improve pattern separation. *Nature* **472**, 466–470 (2011).
28. A. J. Eisch, D. Petrik, Depression and hippocampal neurogenesis: A road to remission? *Science* **338**, 72–75 (2012).
29. M. A. Kheirbek, K. C. Klemm, A. Sahay, R. Hen, Neurogenesis and generalization: A new approach to stratify and treat anxiety disorders. *Nat. Neurosci.* **15**, 1613–1620 (2012).
30. F. Luzzati, S. De Marchis, A. Fasolo, P. Peretto, Neurogenesis in the caudate nucleus of the adult rabbit. *J. Neurosci.* **26**, 609–621 (2006).
31. F. N. Garas *et al.*, Structural and molecular heterogeneity of calretinin-expressing interneurons in the rodent and primate striatum. *J. Comp. Neurol.* **526**, 877–898 (2018).
32. Y. Wu, A. Parent, Striatal interneurons expressing calretinin, parvalbumin or NADPH-diaphorase: A comparative study in the rat, monkey and human. *Brain Res.* **863**, 182–191 (2000).
33. L. Tricoire *et al.*, A blueprint for the spatiotemporal origins of mouse hippocampal interneuron diversity. *J. Neurosci.* **31**, 10948–10970 (2011).
34. M. D. Brandt *et al.*, Transient calretinin expression defines early postmitotic step of neuronal differentiation in adult hippocampal neurogenesis of mice. *Mol. Cell. Neurosci.* **24**, 603–613 (2003).
35. B. Schlösser, G. Klaus, G. Prime, G. Ten Bruggencate, Postnatal development of calretinin- and parvalbumin-positive interneurons in the rat neostriatum: An immunohistochemical study. *J. Comp. Neurol.* **405**, 185–198 (1999).
36. S. Bansod, R. Kageyama, T. Ohtsuka, Hes5 regulates the transition timing of neurogenesis and gliogenesis in mammalian neocortical development. *Development* **144**, 3156–3167 (2017).
37. N. Bertrand, D. S. Castro, F. Guillemot, Proneural genes and the specification of neural cell types. *Nat. Rev. Neurosci.* **3**, 517–530 (2002).
38. I. Imayoshi *et al.*, Roles of continuous neurogenesis in the structural and functional integrity of the adult forebrain. *Nat. Neurosci.* **11**, 1153–1161 (2008).
39. J. Hatakeyama *et al.*, Hes genes regulate size, shape and histogenesis of the nervous system by control of the timing of neural stem cell differentiation. *Development* **131**, 5539–5550 (2004).
40. R. Kageyama, T. Ohtsuka, T. Kobayashi, The Hes gene family: Repressors and oscillators that orchestrate embryogenesis. *Development* **134**, 1243–1251 (2007).
41. M. S. Brill *et al.*, Adult generation of glutamatergic olfactory bulb interneurons. *Nat. Neurosci.* **12**, 1524–1533 (2009).
42. R. D. Hodge, R. J. Kahoud, R. F. Hevner, Transcriptional control of glutamatergic differentiation during adult neurogenesis. *Cell. Mol. Life Sci.* **69**, 2125–2134 (2012).
43. C. Schuurmans *et al.*, Sequential phases of cortical specification involve Neurogenin-dependent and -independent pathways. *EMBO J.* **23**, 2892–2902 (2004).
44. G. Masserdotti, S. Gascón, M. Götz, Direct neuronal reprogramming: Learning from and for development. *Development* **143**, 2494–2510 (2016).
45. F. Guillemot, Cell fate specification in the mammalian telencephalon. *Prog. Neurobiol.* **83**, 37–52 (2007).
46. C. Fode *et al.*, A role for neural determination genes in specifying the dorsoventral identity of telencephalic neurons. *Genes Dev.* **14**, 67–80 (2000).
47. J. M. Tepper *et al.*, Heterogeneity and diversity of striatal GABAergic interneurons: Update 2018. *Front. Neuroanat.* **12**, 91 (2018).
48. D. A. Laplagne *et al.*, Functional convergence of neurons generated in the developing and adult hippocampus. *PLoS Biol.* **4**, e409 (2006).
49. E. Hanson, J. Swanson, B. R. Arenkiel, Sensory experience shapes the integration of adult-born neurons into the olfactory bulb. *J. Nat. Sci.* **3**, e422 (2017).
50. D. O. Dias *et al.*, Reducing pericyte-derived scarring promotes recovery after spinal cord injury. *Cell* **173**, 153–165.e22 (2018).